

# Probing solar modulation of AMS-02 time-dependent D, <sup>3</sup>He and <sup>4</sup>He fluxes with modified force field approximation

CHENG-RUI ZHU<sup>1,2,\*</sup> AND MEI-JUAN WANG<sup>1</sup>

<sup>1</sup>*Department of Physics, Anhui Normal University, Wuhu 241000, Anhui, China*

<sup>2</sup>*Key Laboratory of Dark Matter and Space Astronomy, Purple Mountain Observatory, Chinese Academy of Sciences, Nanjing 210008, Jiangsu, China*

(Dated: February 17, 2025)

## ABSTRACT

The AMS-02 experiment recently published time-dependent fluxes of deuterons (D) from May 2011 to April 2021, divided into 33 periods of four Bartels rotations each. These temporal structures are associated with solar modulation. In this study, three modified force-field approximation are employed to examine the long-term behavior of cosmic-ray (CR) isotopes such as deuteron, <sup>3</sup>He, and <sup>4</sup>He, as well as the ratios D/<sup>3</sup>He and <sup>3</sup>He/<sup>4</sup>He. The solar modulation potential is rigidity-dependent for these modified force-field approximation. Due to the unknown local interstellar spectrum (LIS) for these isotopes, we utilize the Non-LIS method for solar modulation. By fitting to the AMS-02 time-dependent fluxes, we derive the solar modulation parameters. Our findings indicate that all isotopes can be fitted using the same parameters. Thus, the time-independent behavior of the flux ratio at low energy primarily arises from differences in the LIS and the conversion between kinetic energy and rigidity for cosmic rays with varying Z/A ratios. Based on these, we forecast the daily fluxes of D, <sup>3</sup>He and <sup>4</sup>He.

## 1. INTRODUCTION

Galactic cosmic rays (GCRs) originate from cosmic accelerators such as the shocks of supernova remnants and then propagate within the Milky Way (Moskalenko & Strong 1998). However, when they traverse the heliosphere to Earth, they are modulated by the outward-moving magnetized solar wind plasma (Potgieter 2013). Solar modulation is crucial for understanding the nature of GCRs, including their origin (Blasi 2013) and propagation (Strong et al. 2007) within the galaxy. It is also significant for searching for dark matter through low-energy modulated antiproton and antideuteron fluxes (Lavalle & Salati 2012; Cui et al. 2017; Zhu et al. 2022). Previous studies have shown that solar activity influences solar modulation (Usoskin et al. 2011; Potgieter 2013). Stronger solar activities lead to higher levels of solar modulation. The solar modulation exhibits periodicities of 11-year and 22-year cycles corresponding to solar activity periods (Aguilar et al. 2021a, 2022) and daily fluxes show a 27-day cycle corresponding to the solar rotation (Aguilar et al. 2021a, 2022).

To model and predict the intensity of Galactic Cosmic Rays (GCRs), the Parker's transport equation (TPE) (Parker 1965) is employed to depict the propagation processes of cosmic rays within the heliosphere. The Parker's transport equation can be solved by numerical methods or analytical methods. Usually, the force field approximation (FFA) (Gleeson & Axford 1967, 1968) is used to solve the equation as it is simple and enough to explain the observations. However, with the development of instruments, such as PAMELA, AMS-02, and DAMPE (Adriani et al. 2011; Aguilar et al. 2017; Ambrosi et al. 2017), the observation has entered a high-precision era. Although the use of FFA is usually employed for most models of Galactic cosmic rays, it is inadequate to describe the time-dependent GCR spectra themselves as well as the fluxes ratio. Tomassetti et al. (2018); Corti et al. (2019b); Song et al. (2021); Zhu et al. (2022); Wang et al. (2022) reproduced the AMS-02 observations using a one-dimensional or a three-dimensional numerical model respectively to solve the Parker equation. Several methods have been proposed to modify the FFA

\* zhucr@ahnu.edu.cn

((Corti et al. 2016; Zhu et al. 2021; Shen et al. 2021; Long & Wu 2024; Li et al. 2022)) to account for the cosmic rays fluxes.

The recent experimental results have achieved significant breakthroughs that are instrumental in understanding the solar modulation effect as well as the GCRs physics, particularly those from Voyager and AMS-02. So far, only Voyager-1 and Voyager-2 have crossed the boundary of the heliosphere (Stone et al. 2013; Stone et al. 2019) and detected the LIS in the range from a few to hundreds MeV/nucleon. Unfortunately, it is challenging for them to distinguish particle isotopes, which makes it difficult for us to limit the LIS of non-dominant isotopes. The AMS-02 collaboration has published a variety of high-precision cosmic ray spectra (Aguilar et al. 2021b) and the evolution of some cosmic ray fluxes over time (Aguilar et al. 2018a,b).

Very recently, the AMS-02 experiment released the time-dependent fluxes of deuteron (D),  $^3\text{He}$ , and  $^4\text{He}$  (Aguilar et al. 2024) from May 2011 to April 2021, providing new opportunities to study the solar modulation for cosmic rays (CRs). In this study, we employ three modified force field approximations from previous research to investigate the solar modulation of deuterium (D),  $^3\text{He}$ , and  $^4\text{He}$ . It is assumed that each of these modified force-field approximation models incorporates a rigidity-dependent solar modulation potential. In order to study the solar modulation of Galactic Cosmic Rays (GCRs), it is necessary to assume Local Interstellar Spectra (LIS). Typically, Voyager data are used to constrain the LIS. However, the Voyager does not provide data for deuterium (D),  $^3\text{He}$ , and  $^4\text{He}$ . To eliminate the impact of LIS spectra, an alternative method was proposed in (Corti et al. 2019a), referred to here as the Non-LIS method. The results of this study confirm that the MFFA approach represents a valid parameterization of the spectrum for various GCRs. It is of great utility in elucidating the long-term behavior of GCRs and predicting the long-time fluxes of unmeasured GCRs. Based on this assumption, we predict the daily fluxes of D,  $^3\text{He}$  and  $^4\text{He}$  from 2011 to 2020, and most of the total fluxes of  $^3\text{He}$  and  $^4\text{He}$  agree with the measurements of He within their  $1\sigma$  confidence interval.

## 2. METHODOLOGY

### 2.1. Solar Modulation

The existence of heliospheric magnetic field carried by solar winds causes the modulation of GCRs as they enter the heliosphere, resulting in suppressed fluxes of CRs. Above 30 GeV/n (per nucleon) this effect is negligible but it gets increasingly more pronounced at lower energies (Potgieter 2013). The basic transport equation (TPE) was first derived by Parker (Parker 1965; Potgieter 2013) as shown in Eq. 1

$$\begin{aligned} \frac{\partial f}{\partial t} = & -(\vec{V}_{sw} + \langle \vec{v}_D \rangle) \cdot \nabla f + \nabla \cdot (\mathbf{K}^{(s)} \cdot \nabla f) \\ & + \frac{1}{3}(\nabla \cdot \vec{V}_{sw}) \frac{\partial f}{\partial \ln p}. \end{aligned} \quad (1)$$

Here,  $f$  is the cosmic ray distribution function in the phase space  $(\vec{r}, p)$ , and  $p$  denotes momentum. The cosmic ray flux  $J$  measured by experiments is related to the distribution function by  $J \propto p^2 f$ . Particle rigidity  $R$  which is widely used in experimental studies, is related to momentum by  $R = pc/q$ , where  $c$  is the speed of light and  $q$  is the charge of the cosmic ray particles.  $\vec{V}_{sm}$  is the solar wind speed,  $\vec{v}_d$  is the drift velocity and  $\mathbf{K}^{(s)}$  denotes the diffusion tensor. The terms in the right of Eq. 1 describe the convection, drift, diffusion and adiabatic energy loss of GCRs transport effects in the heliosphere. There are various methods to solve the equation and the force-field approximation (FFA) (Gleeson & Axford 1967, 1968) is mostly applied as it is simple enough. In this model, it is assumed that spherical symmetry with (a) a steady state ( $\partial f/\partial t = 0$ ), (b) an adiabatic energy loss rate  $\langle dP/dt \rangle = (P/3)\vec{V}_{sw} \cdot \nabla f/f = 0$ , and (c) no drifts. and we get that the TOA flux is related with the LIS flux as

$$J^{\text{TOA}}(E) = J^{\text{LIS}}(E + \Phi) \times \frac{E(E + 2m_p)}{(E + \Phi)(E + \Phi + 2m_p)}, \quad (2)$$

where  $E$  is the kinetic energy per nucleon,  $\Phi = \phi \cdot Ze/A$  with  $\phi$  being the solar modulation potential,  $m_p = 0.938$  GeV is the proton mass, and  $J$  is the differential flux of GCRs. The only parameter in the force-field model is the modulation potential  $\phi$ .

### 2.2. The Non-LIS method and modified FFA models

Usually, we need the LIS to study the time-dependent solar modulation effects. However we know very very little about the LIS of D,  $^4\text{He}$  and  $^3\text{He}$  as there have been very few experiments to detect these cosmic rays. In order to eliminate the influence of CR LIS, the Non-LIS method is adopted here. If we have two modulated spectral  $J^{TOA}(t_1)$  and  $J^{TOA}(t_2)$ , we get the relation of them from Eq. 2 as (Corti et al. 2019a)

$$J^{TOA}(E, t_1) = J^{TOA}(E + \Delta\Phi, t_2) \times \frac{E(E + 2m_p)}{(E + \Delta\Phi)(E + \Delta\Phi + 2m_p)}. \quad (3)$$

Here,  $\Delta\Phi = \Phi(t_1) - \Phi(t_2) = Ze/A \cdot (\phi(t_1) - \phi(t_2)) = Ze/A \cdot \Delta\phi$ . In this work, we take the mean fluxes from May 2011 to April 2021 as the  $J^{TOA}(t_2)$  (Aguilar et al. 2024). We utilized linear interpolation on a logarithmic scale ( $\log R - \log J$ ) to determine the interpolated flux values for other rigidities that lack observational data.

In principle, the force-field model assumes a quasi-steady-state of the solution of the Parker's equation. However, the observational GCRs fluxes show 11-year variations associated with solar activities. Therefore a time-series of  $\phi$  at different epochs is adopted to describe the data. As with only one parameter, we can not fit the monthly cosmic rays flux very well, rigidity-dependent solar modulation potential is needed (Siruk et al. 2024). In this study, we adopt three modified force-field models. First, we employ the modified force-field model (Zhu's model) from Zhu (2024), which is an extension of the model presented in Corti et al. (2016); Gieseler et al. (2017). The solar modulation potential is

$$\Delta\phi(R)_{Zhu} = \phi_l + \left( \frac{\phi_h - \phi_l}{1 + e^{(-R+R_b)}} \right), \quad (4)$$

where  $\phi_l$  is the solar modulation potential for the low energy, and  $\phi_h$  is for the high energy,  $e$  is the natural constant,  $R$  is the rigidity and  $R_b$  is the break rigidity. The sigmoid function is employed here to smooth the transition.  $\phi_l$ ,  $\phi_h$  and  $R_b$  are the free parameters to be fitted. Second, we take the Cholis' model from Cholis et al. (2016); Cholis et al. (2022) as

$$\Delta\phi(R)_{Cholis} = \phi_0 + \phi_1 \left( \frac{1 + (R/R_0)^2}{\beta(R/R_0)^3} \right). \quad (5)$$

Here,  $\beta$  is the ratio between the particle speed and the speed of light.  $\phi_1$ ,  $\phi_2$  and  $R_0$  are the free parameters to be fitted. Third, we take Long's model from Long & Wu (2024) as

$$\Delta\phi(R)_{Long} = \phi_0 + \phi_1 \ln(R/R_0), \quad (6)$$

with

$$J^{TOA}(E, t_1) = J^{TOA}(E + \Delta\Phi, t_2) \times \frac{E(E + 2m_p)}{(E + \Delta\Phi)(E + \Delta\Phi + 2m_p)} \exp\left(-g \frac{10R^2}{1 + 10R^2} \Delta\phi\right). \quad (7)$$

Here,  $\phi_0$ ,  $\phi_1$  and  $g$  are the free parameters to be fitted. Shen et al. (2021) presents Shen's model. However, to achieve better fitting results for different cosmic-ray species, it is necessary to modify the model to be rigidity dependent rather than energy dependent. Therefore, we do not employ their model in this work.

### 2.3. MCMC

We fit the three solar modulation  $\phi(R)$  with three free parameters. The  $\chi^2$  statistics is defined as

$$\chi^2 = \sum_{i=1}^m \frac{[J(E_i; \phi(R)) - J_i(E_i)]^2}{\sigma_i^2}, \quad (8)$$

where  $J(E_i; \phi(R))$  is the expected modulated flux,  $J_i(E_i)$  and  $\sigma_i$  are the measured flux and error for the  $i$ th data bin with the geometric mean of the bin edges as  $E_i$ .

We use the Markov Chain Monte Carlo (MCMC) algorithm to minimize the  $\chi^2$  function, which works in the Bayesian framework. The posterior probability of model parameters  $\theta$  is given by

$$p(\theta|\text{data}) \propto \mathcal{L}(\theta)p(\theta), \quad (9)$$

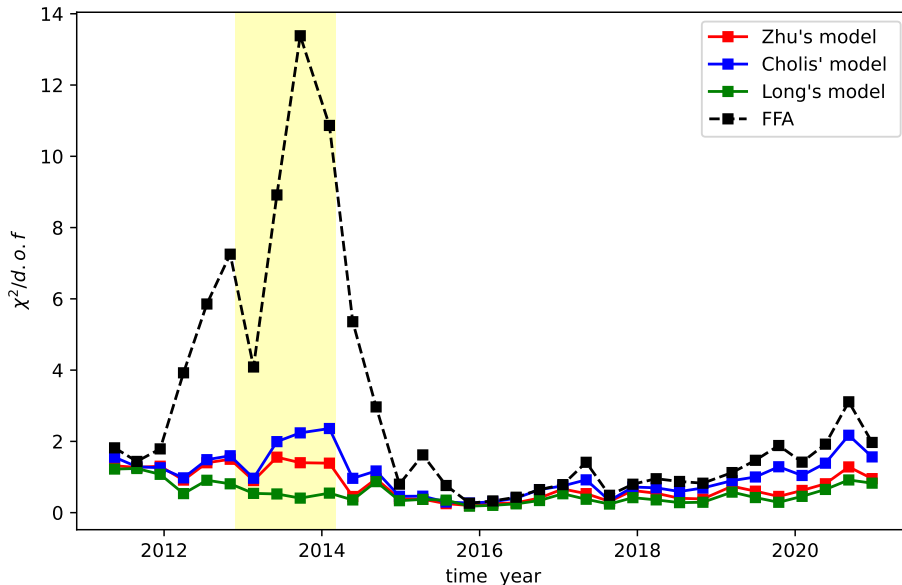


**Figure 1.** The figure illustrates  $\chi^2/d.o.f$  values for the four models for the combined analysis ( $D+{}^3\text{He}+{}^4\text{He}$ ). Specifically, the blue curve corresponds to Zhu’s model, the red curve represents Cholis’ model, and the green curve denotes Long’s model. The FFA result is depicted in black for comparison. The yellow shaded band stands for the heliospheric magnetic field reversal period within which the polarity is uncertain (Sun et al. 2015).

where  $\mathcal{L}(\theta)$  is the likelihood function of parameters  $\theta$  given the observational data, and  $p(\theta)$  is the prior probability of  $\theta$ .

The MCMC driver is adapted from CosmoMC (Lewis & Bridle 2002; Liu et al. 2012). We adopt the Metropolis-Hastings algorithm. The basic procedure of this algorithm is as follows. We start with a random initial point in the parameter space, and jump to a new one following the covariance of these parameters. The accept probability of this new point is defined as  $\min[p(\theta_{\text{new}}|\text{data})/p(\theta_{\text{old}}|\text{data}), 1]$ . If the new point is accepted, then repeat this procedure from this new one. Otherwise go back to the old point. For more details about the MCMC one can refer to (Gelman 1997).

### 3. RESULTS AND DISCUSSION

We have jointly fitted the time-dependent spectra of deuterium,  ${}^3\text{He}$ , and  ${}^4\text{He}$  from AMS-02 together with FFA and three modified FFA models. The time dependent  $\chi^2/d.o.f$  values are shown in Fig. 1. It is noteworthy that the degrees of freedom (d.o.f) for the FFA are 77, whereas for the three modified FFA models, they amount to 75. It is evident that the three modified FFA models significantly reduce the  $\chi^2/d.o.f$  during the period of heliospheric magnetic field reversal, where the polarity remains uncertain. Meanwhile, the FFA continues to provide adequate predictions during the solar minimum from 2015 to 2021. Upon comparing the three modified FFA models, we find that Long’s model yields the best fitting results, with  $\chi^2/d.o.f$  values ranging from 0.182 to 1.239 and a mean value of 0.537. Zhu’s model provides  $\chi^2/d.o.f$  values ranging from 0.202 to 1.557 and a mean value of 0.771. Meanwhile, Cholis’ model gives  $\chi^2/d.o.f$  values ranging from 0.270 to 2.361 and a mean value of 1.054.

In Fig. 2, we show the  $\chi^2$  results of the four models for independent analysis of D,  ${}^3\text{He}$  and  ${}^4\text{He}$ , as well as the combined analysis respectively. The specific values are shown in Table. 1, 2, 3 and 4 in the appendix. Similar to the combine analysis, the FFA is particularly poor to simulate the solar modulation during the heliosphere magnetic field reversal period for the independent analysis. So that we need a more reliable model to study the propagation of Galactic cosmic rays. As the relative error of the D flux is 2 to 3 times that of  ${}^3\text{He}$  and  ${}^4\text{He}$ , the deuterium gets better fitting results than He isotopes. It means that for more precise data, we may need a more refined and physically motivated model. However, for now, the Zhu and Long’s models are sufficient because the average  $\chi^2/d.o.f$  value is smaller than 1.

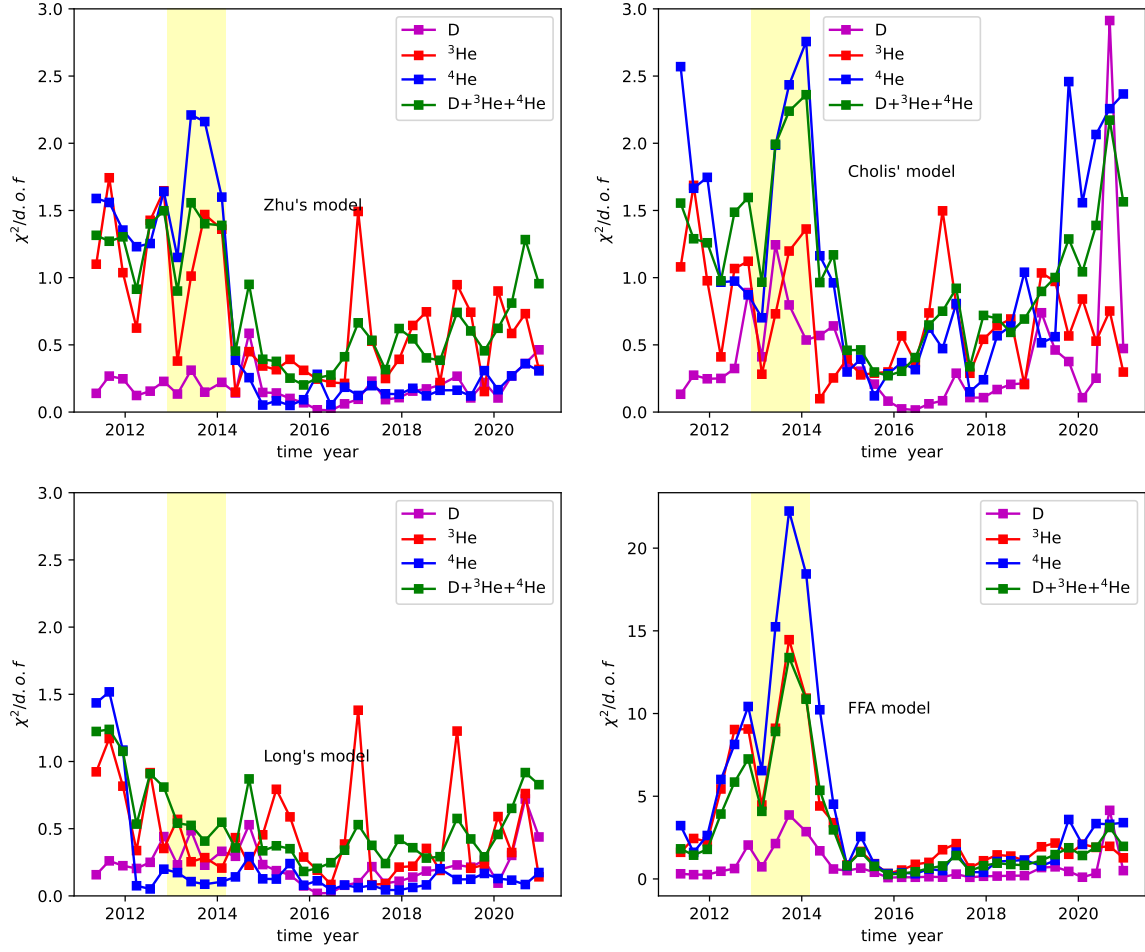


**Figure 2.** The  $\chi^2/d.o.f$  over time for the analysis of each independent isotope (D,  $^3\text{He}$  or  $^4\text{He}$ ), as well as the combined analysis ( $\text{D}+^3\text{He}+^4\text{He}$ ), for the Zhu's model (top left), the Cholis' model (top right), the Long's model (bottom left) and the FFA model (bottom right). In the FFA model, the degrees of freedom ( $d.o.f$ ) are 25 for the analysis of each independent isotope and 77 for the combined analysis. As for the other three models, the  $d.o.f$  are 23 for the analysis of each independent isotope and 75 for the combined analysis. The yellow shaded band stands for the heliospheric magnetic field reversal period within which the polarity is uncertain (Sun et al. 2015).

In Fig. 3, we show the model prediction proton fluxes from 2011-05-20 to 2011-08-30, from 2014-02-07 to 2014-05-2 and from 2017-05-10 to 2017-08-25 respectively with the same parameters from the fitting in the manuscript with four models. The  $J^{TOA}(t_2)$  in the Eq.3 here is derived from the  $\Phi_D/(\text{ratio of D to p})$  from (Aguilar et al. 2024). We get the  $\Phi_p$  for each time interval reported in Aguilar et al. (2024), then derived the average value of  $\Phi_p$ , which we designate as  $J^{TOA}(t_2)$ . The point data is taken from the mean fluxes of AMS-02 daily protons fluxes (Aguilar et al. 2021a) in the same period. Note that the proton publication of Aguilar et al. (2021a) includes the D flux, i.e. p+D, in this paper the D component is not excluded. During the heliospheric magnetic field reversal period, within which the polarity is uncertain, Long's model gives the best prediction results, followed by Zhu's and Cholis' models. The FFA result is far away from the measurement. For the three modified models, the predicted proton fluxes correspond to the measurements within about 3% for most cases.

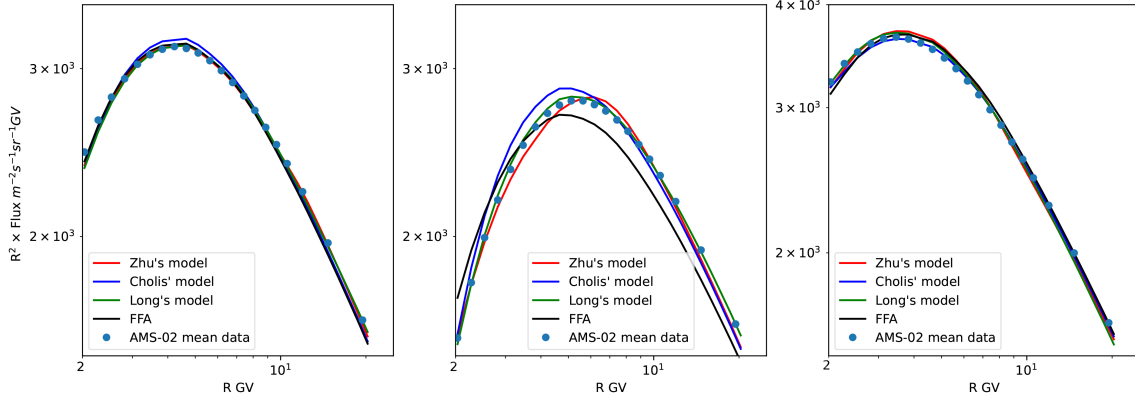


**Figure 3.** The model prediction proton fluxes from 2011-05-20 to 2011-08-30, from 2014-02-07 to 2014-05-2 and from 2017-05-10 to 2017-08-25 respectively with the same parameters from the fitting in the manuscript. The  $J^{TOA}(t_2)$  in the Eq.3 here is derived from the  $\Phi_D/(\text{ratio of D to p})$  from (Aguilar et al. 2024). The point data is taken from the mean fluxes of AMS-02 daily protons fluxes (Aguilar et al. 2021a) in the same period. Note that the Y-axis represents the flux, which we have re-scaled using the  $R^2$  (Lafferty & Wyatt 1995)

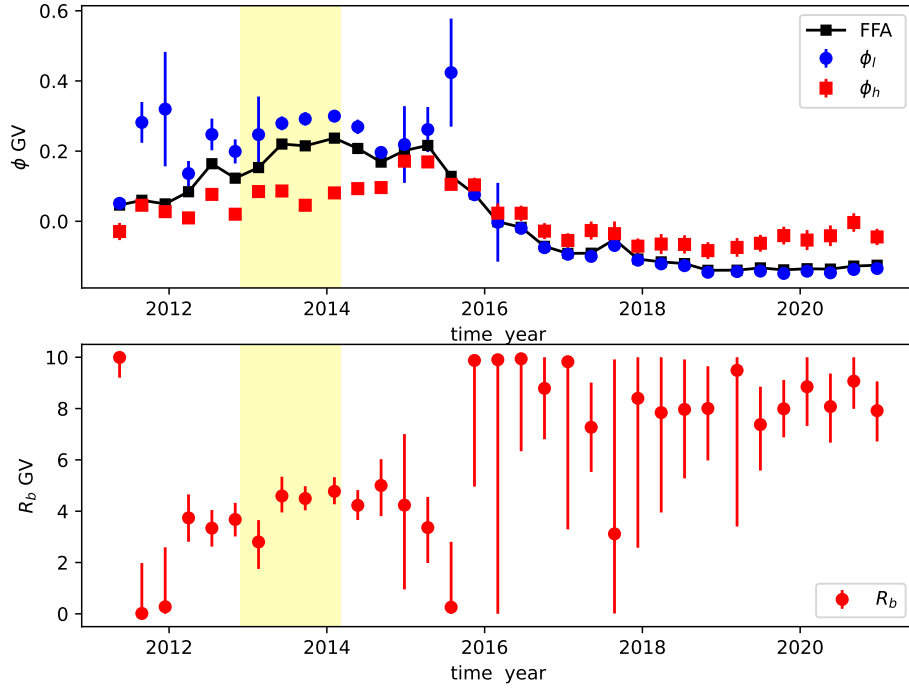


**Figure 4.** The fitting results of Zhu's model. (Top) Time series of  $\phi_l$  (blue) and  $\phi_h$  (red) via fitting to the AMS-02 data. The solar modulation potentials from the FFA (black) are shown for comparison. (Bottom) Same to the top but for  $R_b$ . The shaded band stands for the heliospheric magnetic field reversal period within which the polarity is uncertain.

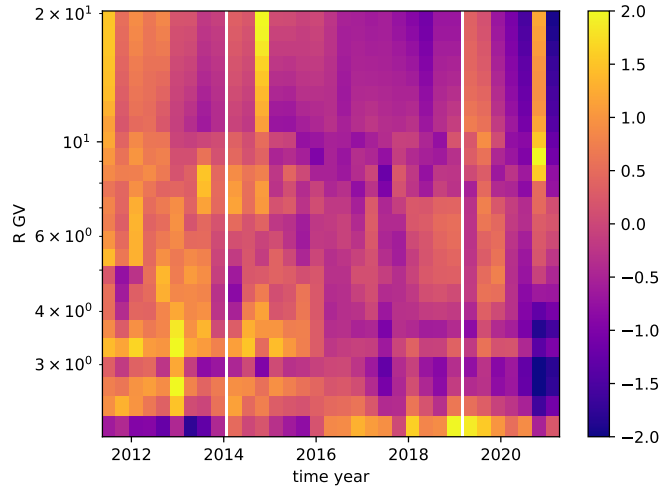


**Figure 5.** Zhu’s model prediction comparing to the data ( $\frac{J_{model}-J_{data}}{\sigma_{data}}$ ) of D from May 2011 to April 2021.

All the three modified models incorporate a rigidity-dependent solar modulation potential and yield very good fitting results. Although the Long’s model gets the best fitting results, it may not be suitable to extend to high rigidity. The scale index  $g$  potentially exerts a consistent and uniform influence across all rigidity ranges, essentially resembling a rescaling of the LIS, where it efficiently allocates distinct LIS values to varying epochs. In this work, we find that the Cholis’ model is only slightly worse than Zhu’s model. However, (Long & Wu 2024) shows that Cholis’ model performs poorly in simulating the solar modulation for proton and helium fluxes, particularly during the solar reversal phase. As the rigidity range of deuterium,<sup>3</sup> He, and <sup>4</sup>He is 2 to 20 GV, while the rigidity range for proton and helium is 1 to 60 GV, this may indicate that the Cholis’ model is only suitable for a narrower rigidity range.

The main reason of rigidity-dependence of solar modulation potential is the break in the diffusion coefficients. The typical empirical expression of diffusion coefficients used in numerical are broken power-law, where  $a$  for the slope of the power law at low rigidities and  $b$  for the slope of the power law at high rigidities (Potgieter et al. 2014). (Potgieter et al. 2014, 2015; Di Felice et al. 2017; Luo et al. 2019; Song et al. 2021) modeled the time-dependent GCRs spectra by adjusting the diffusion coefficients with time. The different slope of the power law at low and high rigidities will induce a rigidity-dependent solar modulation behavior and the modified FFA models here can empirically describe this behavior.

The fitting parameters for Zhu’s model are shown in Fig. 4. In the bottom panel of Fig. 4, we present the time-series of  $R_b$ . The mean value of  $R_b$  is 6.03 GV, corresponding to the result of Zhu (2024) within  $2\sigma$  confidence intervals. Notably, if the value of  $R_b$  is excessively low, it implies that the potential transition range will be more significant in the low energy region, rather than being dependent on  $\phi_l$ . The time-series of  $\phi_l$  and  $\phi_h$  are displayed in the top panel of Fig. 4. The fluctuation of  $\phi_h$  is relatively small, with a mean value of 0.014 GV, ranging from  $-0.085$  GV to 0.174 GV. This is because high energy particles are less influenced by solar modulation.

Around 2016, the value of  $\phi_l$  approaches  $\phi_h$ , indicating that the FFA is sufficient to explain solar modulation and the break is not obvious, so that the parameter  $R_b$  is not important. The model indeed shows signs of overfitting here. These overfitting means that we only need one parameter to describe the solar modulation here, and the solar modulation potential seems to be rigidity-independent. But we should notice that we use the none LIS solar modulation model here, which means the solar modulation rigidity-dependence around 2016 should be same or similar to the solar modulation potential of  $J^{TOA}(t_2)$  used in the paper.

In Fig. 5, 6, 7, we present the ratios of Zhu’s model-predicted intensities to measured values for D, <sup>3</sup>He and <sup>4</sup>He, respectively. It is evident that most of the fits align with the data within a  $2\sigma_{data}$  margin, utilizing the same solar modulation parameters.

We show the fitting parameters for Long’s model in Fig. 8. Before 2016,  $\phi_1$  is less than zero, and after 2016,  $\phi_1$  is greater than zero. So the rigidity-dependence is similar to the Zhu’s model. In Fig. 9, 10, and 11, we show the Long’s model predictions compared to measurements. Here we can see that Long’s model is slightly better than Zhu’s model.

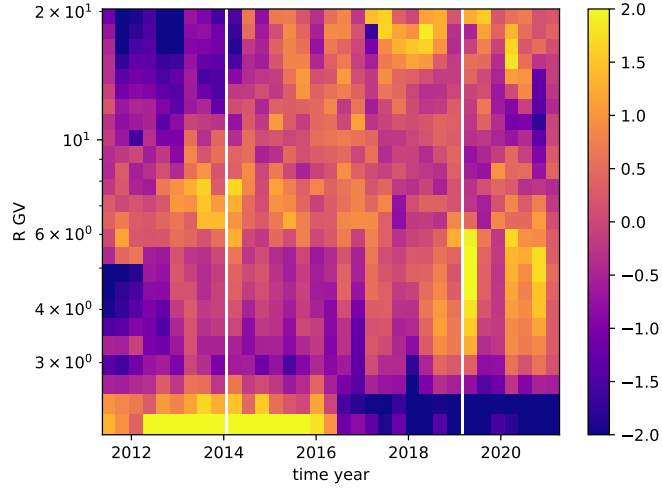


**Figure 6.** Zhu's model prediction comparing to the data ( $\frac{J_{model}-J_{data}}{\sigma_{data}}$ ) of  $^3\text{He}$  from May 2011 to April 2021.

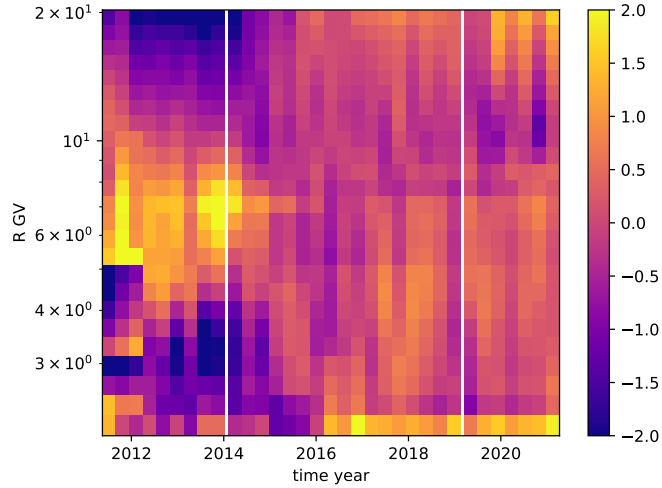


**Figure 7.** Zhu's model prediction comparing to the data ( $\frac{J_{model}-J_{data}}{\sigma_{data}}$ ) of  $^4\text{He}$  from May 2011 to April 2021.

In Fig. 12 13, we show the fluxes ratio of D to  $^4\text{He}$  and  $^3\text{He}$  to  $^4\text{He}$  at rigidities = 2.032 GV, 2.531 GV, 3.825 GV and 20.28 GV, respectively. The Zhu's model predictions are marked with magenta lines and the Long's model results are marked with cyan lines. Please note that the flux ratios are not used in the fitting. The model predictions show that there is nearly no any time-dependent in the fluxes ratio of D to  $^4\text{He}$ , except at the very low rigidities. While there is a clear time dependence below 3GV for the fluxes ratio of  $^3\text{He}$  to  $^4\text{He}$ . It appears that the model cannot reproduce the  $^3\text{He}/^4\text{He}$  ratio at low rigidities; however, the difference between the model and the data is no more than 7%.

According to the Eq. 2, the flux ratio of particles  $a$  and  $b$  can be expressed as:

$$\begin{aligned} \frac{J_a^{TOA}(R^{TOA})}{J_b^{TOA}(R^{TOA})} &= \frac{J_a^{TOA}(E_a^{TOA})(\frac{Z\beta}{A})_a}{J_b^{TOA}(E_b^{TOA})(\frac{Z\beta}{A})_b} \\ &= \frac{(\frac{Z\beta}{A})_a J_a^{LIS}(E_a^{LIS})}{(\frac{Z\beta}{A})_b J_b^{LIS}(E_b^{LIS})} \left( \frac{R_b^{LIS}}{R_a^{LIS}} \right)^2. \end{aligned} \quad (10)$$



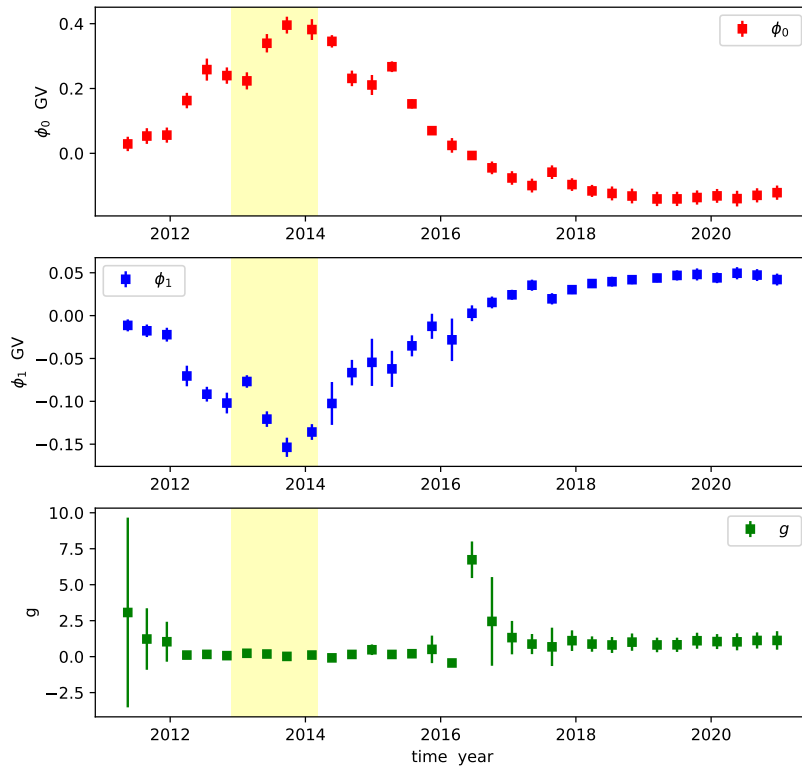


**Figure 8.** The fitting results of Long’s model. (Top) Time series of  $\phi_0$ . (Middle) Time series of  $\phi_1$ . (Bottom) Same to the top but for  $g$ . The shaded band stands for the heliospheric magnetic field reversal period within which the polarity is uncertain.

Here,  $E^{TOA} = E^{LIS} - \frac{Ze}{A}\phi(R)$ , and  $E = \sqrt{R^2(\frac{Ze}{A})^2 + m_0^2} - m_0$ . As the particles have different LIS and  $Z/A$  values, the long-term behavior of the fluxes ratio mainly arises from the second and third terms of Eq. 10 with the same time series of  $\phi(R)$ . Because  $^3\text{He}$  and  $^4\text{He}$  have different  $Z/A$  and LIS, the time dependency in the fluxes ratio will be more obvious. D and  $^4\text{He}$  possess distinct Local Interstellar Spectra (LIS) shapes, attributed to their varied origins (Cooke et al. 2018; Yuan & Fan 2024). Consequently, even though they share the same  $Z/A$ , the ratio of D to  $^4\text{He}$  could exhibit time dependency in the lower rigidity ranges. This discrepancy highlights the significant influence of LIS on particle fluxes. Similarly, helium exhibits a different LIS compared to carbon and oxygen, whereas carbon and oxygen display remarkably similar LIS (Zhu et al. 2018). This disparity will result in the He/O ratio showing time dependency at low rigidities, while the C/O ratio remains time-independent. However, the long-term behavior will be beyond the detection capabilities of AMS-02 (Aguilar et al. 2025).

In our previous work (Zhu & Wang 2025), we obtained the daily solar modulation parameters for p and He. Consequently, we can use these parameters to forecast the daily fluxes of D,  $^3\text{He}$  and  $^4\text{He}$ . First, we need the LIS of these three particles, as the parameters from (Zhu & Wang 2025) are deduced with LIS. We assume that the mean fluxes of D,  $^3\text{He}$  and  $^4\text{He}$  from 2011/5/20 to 2018/3/29 have the same solar modulation potential as the 7-year period fluxes of p and He (Aguilar et al. 2021b), which is 0.477 GV. Then we can calculate the daily fluxes of them after getting the LIS with the solar modulation parameters. As Long’s and Zhu’s model is better, and they give similar results (Zhu & Wang 2025; Zhu & Duan 2025), we show the forecasted results of Zhu’s model in Fig. 14, 15 and 16. The forecasted results are in good agreement with the measurements. In Fig. 17, we show the  $^3\text{He}$  fluxes plus  $^4\text{He}$  fluxes comparing

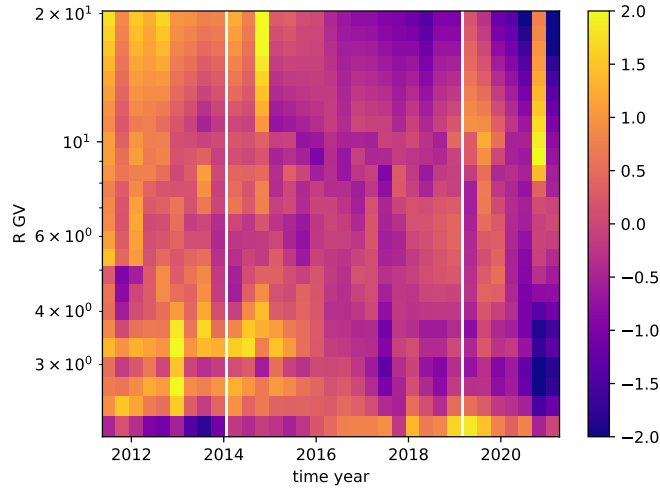


**Figure 9.** Long’s model prediction comparing to the data ( $\frac{J_{model}-J_{data}}{\sigma_{data}}$ ) of D from May 2011 to April 2021.

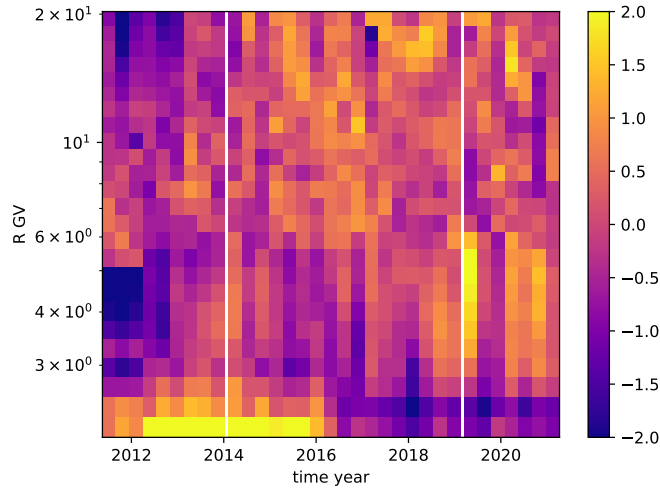


**Figure 10.** Long’s model prediction comparing to the data ( $\frac{J_{model}-J_{data}}{\sigma_{data}}$ ) of  ${}^3\text{He}$  from May 2011 to April 2021.

to the daily measurement of He from 2011 to 2020. are consistent with the data within the  $1\sigma$  confidence interval. For more forecasting results in the range of 2 to 20 GV, please visit our homepage<sup>1</sup>.

#### 4. CONCLUSION

The precise measurement of cosmic ray (CR) spectra is crucial for understanding solar modulation. It also offers a valuable opportunity to enhance our comprehension of CR propagation and to explore new frontiers in astrophysics, and perhaps even uncover new physical phenomena. In this study, we examine the solar modulation of the recently observed time-dependent fluxes of D,  ${}^3\text{He}$ , and  ${}^4\text{He}$  using data from AMS-02 (Aguilar et al. 2024) and employing different modified FFA models. Instead of using a constant solar modulation potential as in the FFA, they all introduce a rigidity-dependent solar modulation potential  $\phi(R)$ . Given the current limited understanding of the LIS for these isotopes, we adopt a non-LIS method in our analysis. All the three models can achieve excellent fits to the data using

<sup>1</sup> <https://github.com/zhucr/daily-fluxes-of-D-He3-He4.git>

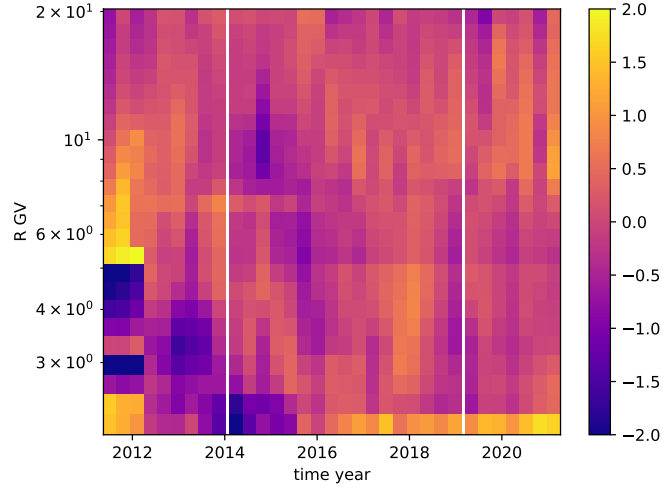


**Figure 11.** Long's model prediction comparing to the data ( $\frac{J_{model}-J_{data}}{\sigma_{data}}$ ) of  $^4\text{He}$  from May 2011 to April 2021.

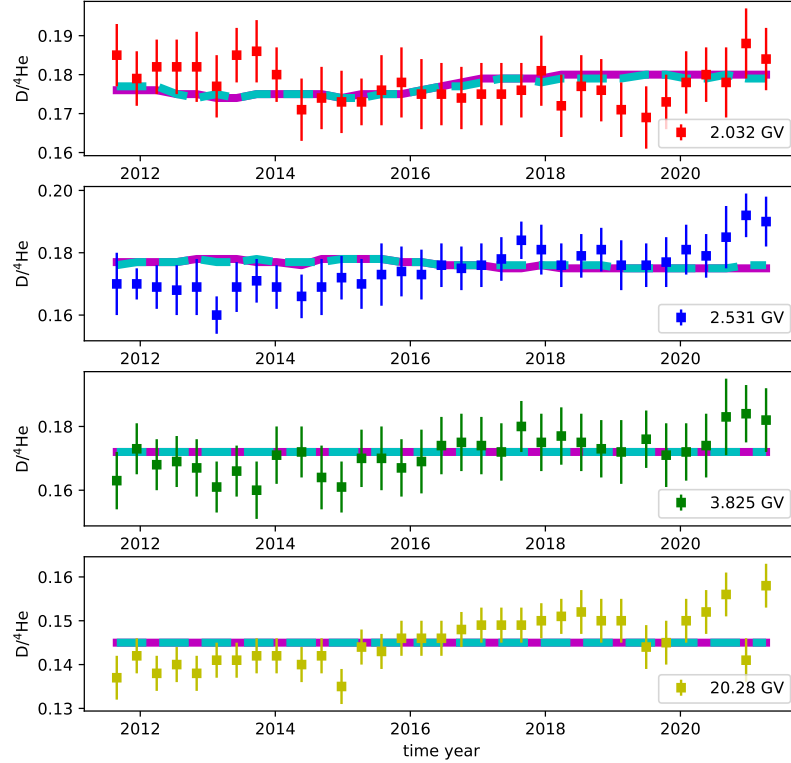


**Figure 12.** Zhu's model prediction (magenta line) and Long's model prediction (cyan line) of  $D/^4\text{He}$  fluxes ratio comparing to the data from May 2011 to April 2021 at rigidities = 2.032 GV, 2.531 GV, 3.825 GV and 20.28 GV.

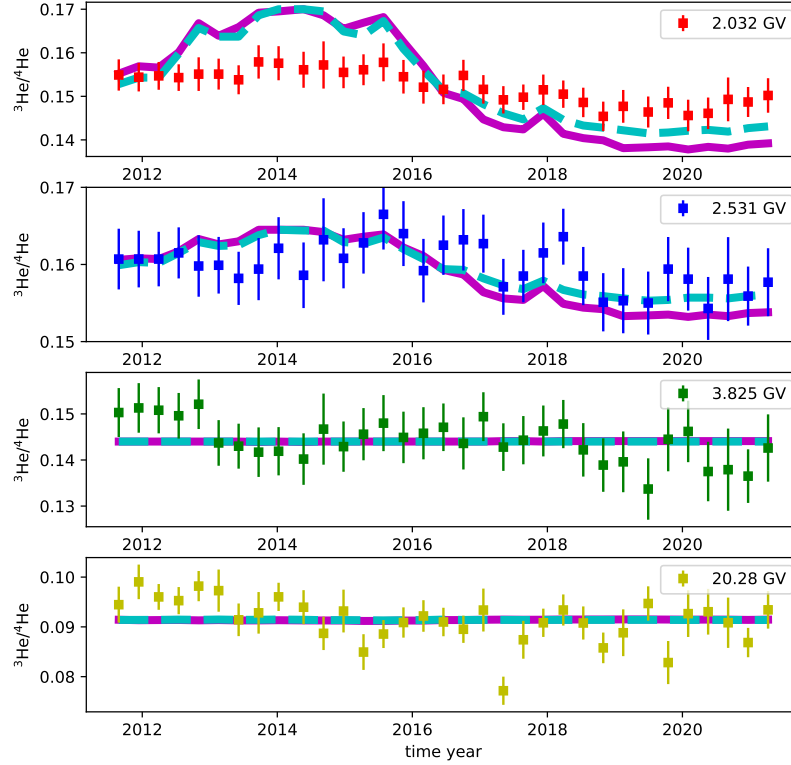


**Figure 13.** Zhu’s model prediction (magenta line) and Long’s model prediction (cyan line) of  ${}^3\text{He}/{}^4\text{He}$  fluxes ratio comparing to the data from May 2011 to April 2021 at rigidities = 2.032 GV, 2.531 GV, 3.825 GV and 20.28 GV.

consistent parameters. Long’s model yields the best fitting results with a mean  $\chi^2/d.o.f$  value of 0.537. Following that is Zhu’s model, which has a mean  $\chi^2/d.o.f$  value of 0.771. The Cholis’ model provides the highest mean  $\chi^2/d.o.f$  value at 1.053.

Combining previous results (Tomassetti et al. 2018; Song et al. 2021; Wang et al. 2022; Long & Wu 2024; Zhu 2024), where they fit the proton and Helium fluxes with the same solar modulation parameters, we can achieve excellent fits to the data using consistent parameters across all these isotopes, indicating that these CRs undergo similar propagation processes within the heliosphere. These facts may indicate that all positively charged CRs undergo the same propagation processes, meaning they all have a universal mean free path. This assumption also works for the negative particles. In Zhu & Duan (2025), we predicted the daily fluxes of antiproton, and the subsequent AMS-02 results indicate that the forecasts are in agreement with the measurements within the  $1\sigma$  confidence interval. In this work, we forecast the daily fluxes of D,  ${}^3\text{He}$  and  ${}^4\text{He}$  following the work Zhu & Duan (2025). The future time-dependent data from AMS-02 will provide further validation for this assumption.

The time-dependent behaviors of flux ratios at low energies, where the isotopes share the same solar modulation parameters, can be attributed to two main factors:  $Z/A$  and LIS. For instance,  ${}^3\text{He}$  and  ${}^4\text{He}$  exhibit different  $Z/A$  values and LIS shapes, leading to a time-dependent  ${}^3\text{He}/{}^4\text{He}$  flux ratio below 3 GV. Similarly, D and  ${}^4\text{He}$  have distinct LIS shapes, resulting in time-dependent behavior of the D/ ${}^4\text{He}$  flux ratio below 4.5 GV, despite their identical  $Z/A$  values.

These models are based on a series of assumptions, such as we do not consider the difference in modulation effect from  $Z/A$ , which may cause hysteresis between the helium-to-proton flux ratio and the helium flux. This will be further studied in our future work. As the modified FFA models can give very good fitting results, it will be useful for studying the origin and propagation of GCRs in the galaxy.

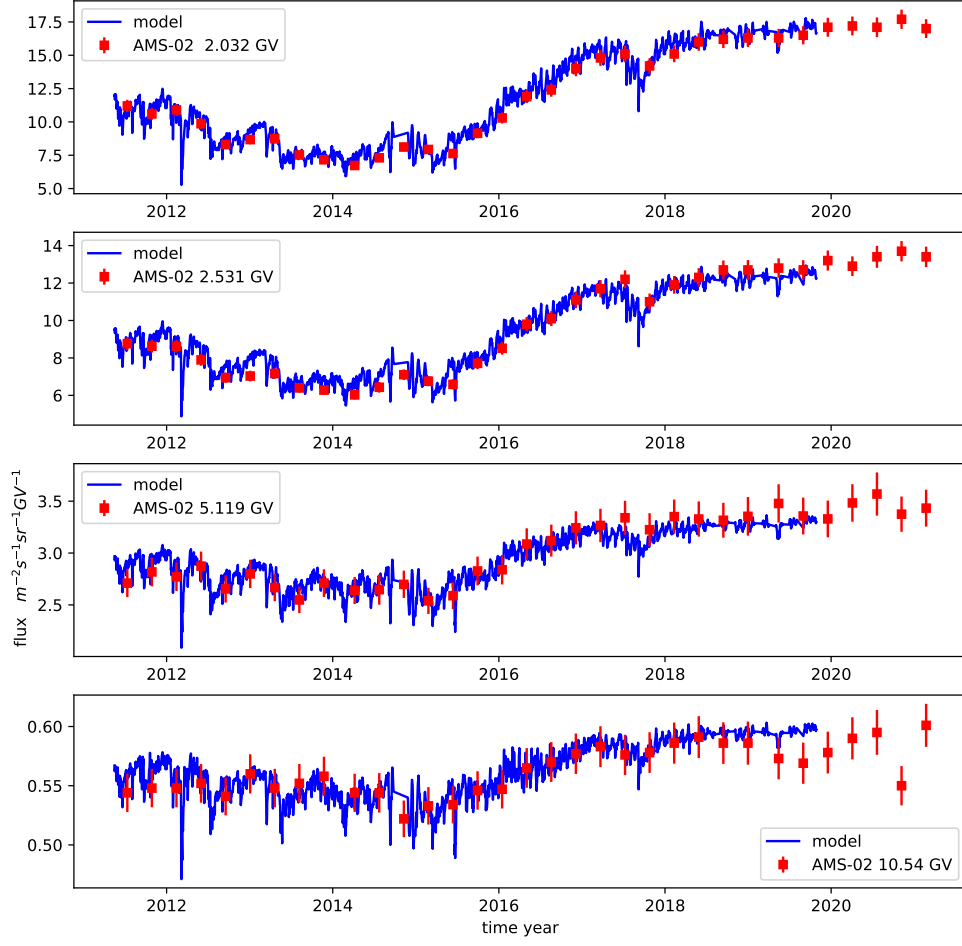


**Figure 14.** Zhu's model prediction of D daily fluxes (blue lines) to the data from May 2011 to April 2021 at rigidities = 2.032 GV, 2.531 GV, 5.119 GV and 10.54 GV.

- 1 Thanks to Fan Yi-Zhong, Yuan Qiang for very helpful discussions. This work is supported by the National Natural
- 2 Science Foundation of China (No. 12203103). Z.C.R is also supported by the Doctoral research start-up funding of
- 3 Anhui Normal University. We acknowledge the use of data from the [AMS Publications](#) .

## APPENDIX

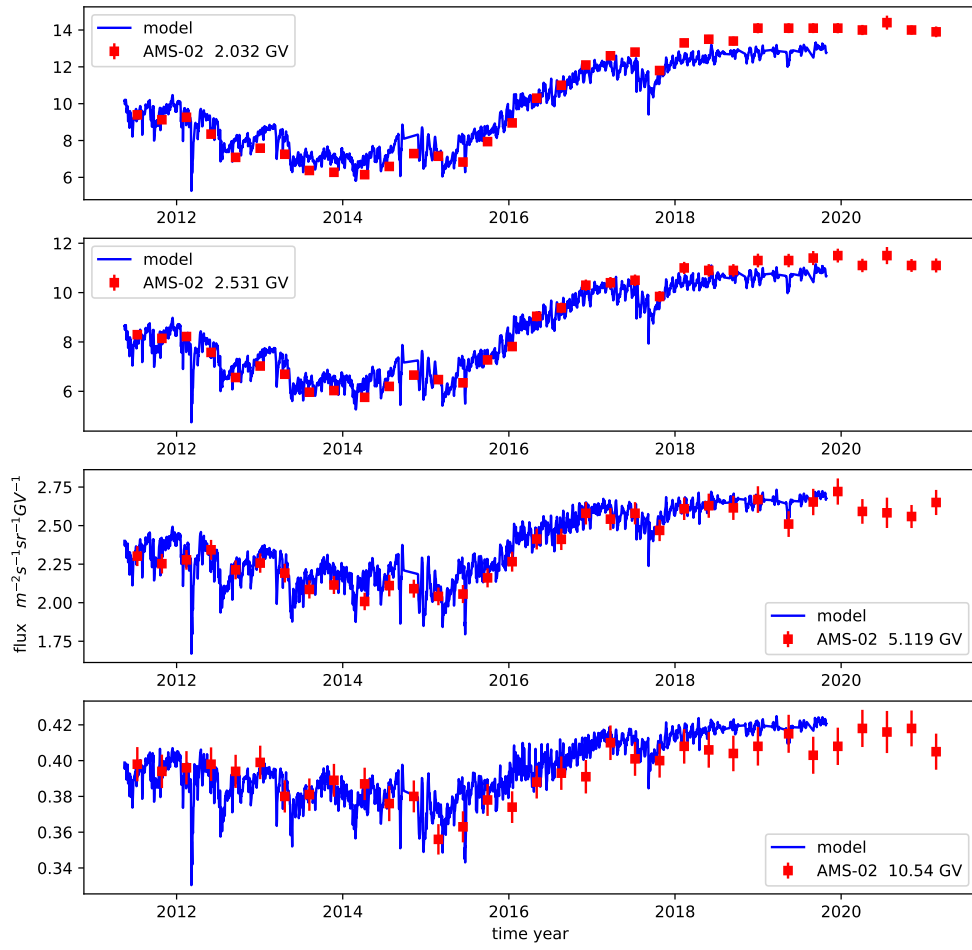


**Figure 15.** Zhu's model prediction of  ${}^3\text{He}$  daily fluxes (blue lines) to the data from May 2011 to April 2021 at rigidities = 2.032 GV, 2.531 GV, 5.119 GV and 10.54 GV.

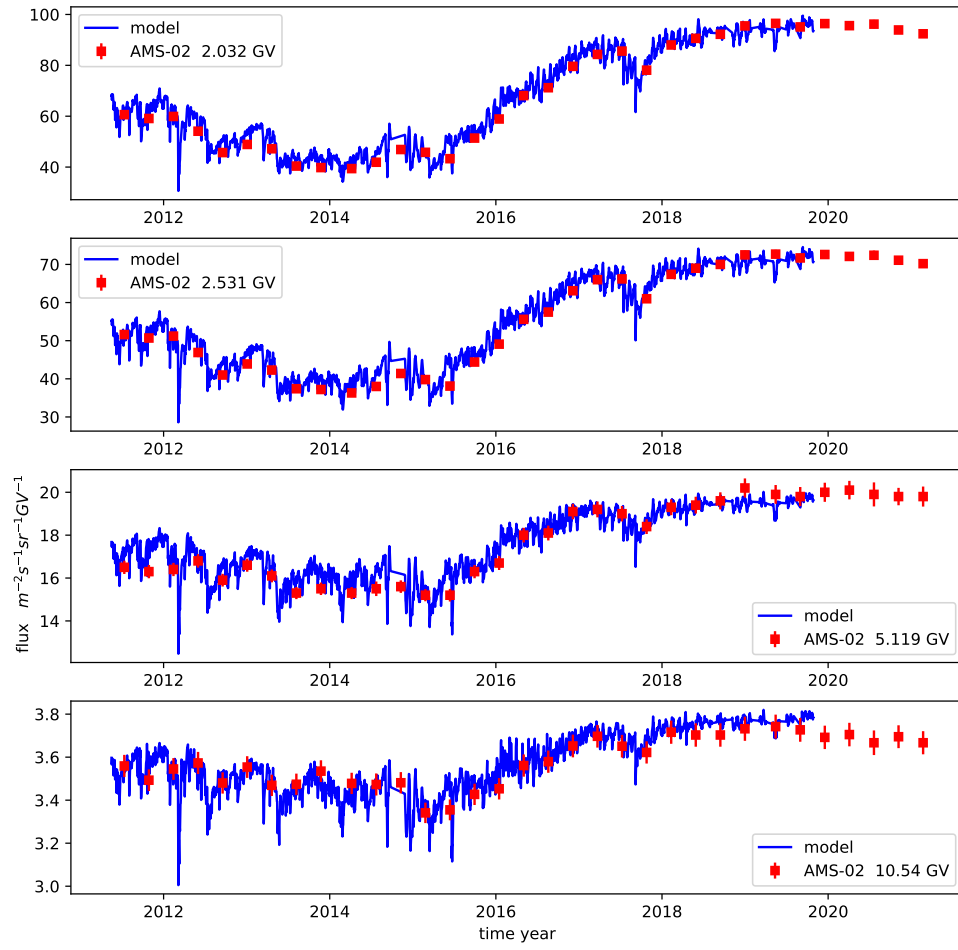


**Figure 16.** Zhu's model prediction of  ${}^4\text{He}$  daily fluxes (blue lines) to the data from May 2011 to April 2021 at rigidities = 2.032 GV, 2.531 GV, 5.119 GV and 10.54 GV.

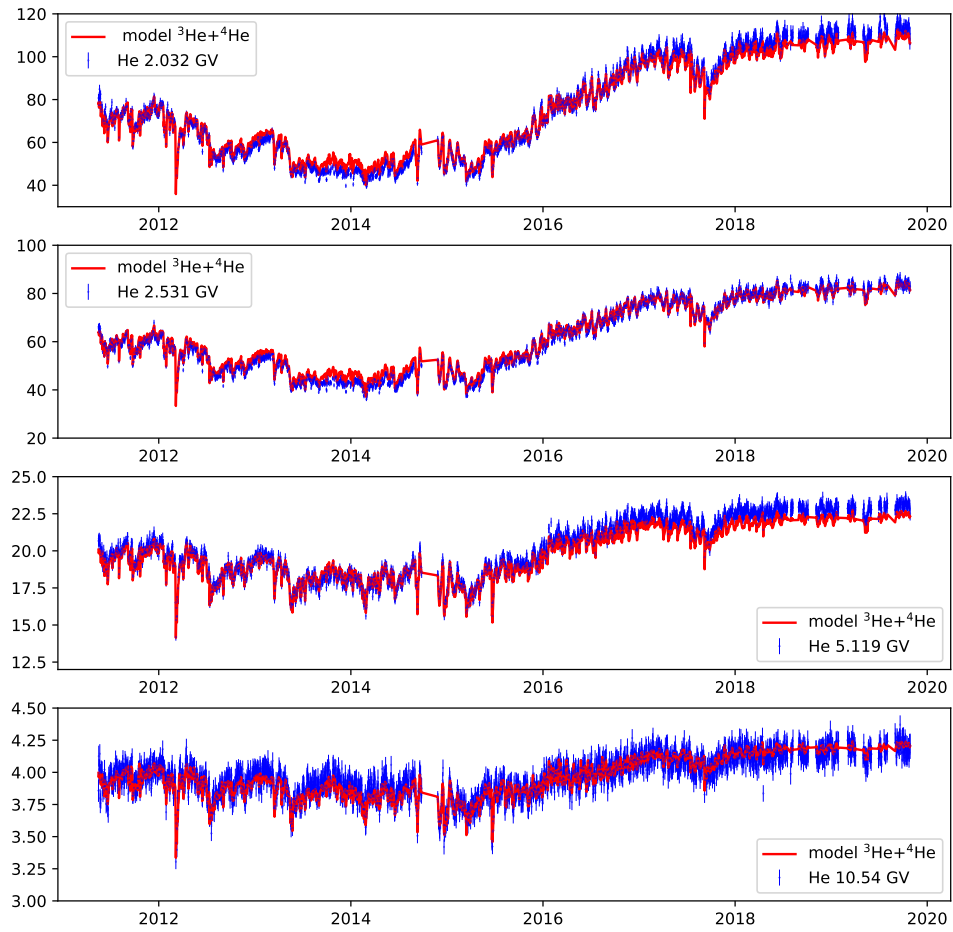


**Figure 17.** Zhu's model prediction of  ${}^3\text{He} + {}^4\text{He}$  daily fluxes (blue lines) to the data from May 2011 to April 2020 (Aguilar et al. 2022) at rigidities = 2.032 GV, 2.531 GV, 5.119 GV and 10.54 GV.



begin date	end date	D	<sup>3</sup> He	<sup>4</sup> He	D+ <sup>3</sup> He+ <sup>4</sup> He
2011-05-20	2011-08-30	0.139	1.100	1.589	1.315
2011-08-31	2011-12-16	0.268	1.743	1.560	1.271
2011-12-17	2012-04-02	0.247	1.037	1.354	1.304
2012-04-03	2012-07-19	0.123	0.625	1.231	0.914
2012-07-20	2012-11-04	0.156	1.427	1.254	1.400
2012-11-05	2013-02-20	0.228	1.646	1.641	1.498
2013-02-21	2013-06-08	0.134	0.379	1.151	0.900
2013-06-09	2013-09-24	0.312	1.012	2.210	1.557
2013-09-25	2014-01-10	0.148	1.470	2.161	1.401
2014-02-07	2014-05-25	0.221	1.361	1.599	1.389
2014-05-26	2014-09-10	0.142	0.148	0.386	0.454
2014-09-11	2014-12-27	0.586	0.449	0.256	0.950
2014-12-28	2015-04-14	0.146	0.343	0.052	0.393
2015-04-15	2015-07-31	0.142	0.315	0.083	0.377
2015-08-01	2015-11-16	0.101	0.392	0.050	0.253
2015-11-17	2016-03-03	0.069	0.311	0.092	0.202
2016-03-04	2016-06-19	0.017	0.245	0.281	0.254
2016-06-20	2016-10-05	0.013	0.221	0.054	0.275
2016-10-06	2017-01-21	0.061	0.213	0.185	0.412
2017-01-22	2017-05-09	0.095	1.493	0.124	0.664
2017-05-10	2017-08-25	0.230	0.527	0.196	0.534
2017-08-26	2017-12-11	0.092	0.250	0.136	0.316
2017-12-12	2018-03-29	0.107	0.393	0.133	0.621
2018-03-30	2018-07-15	0.156	0.644	0.177	0.545
2018-07-16	2018-10-31	0.172	0.746	0.120	0.403
2018-11-01	2019-02-16	0.201	0.220	0.162	0.385
2019-03-16	2019-07-01	0.267	0.948	0.163	0.742
2019-07-02	2019-10-17	0.105	0.743	0.120	0.603
2019-10-18	2020-02-02	0.220	0.153	0.308	0.456
2020-02-03	2020-05-20	0.105	0.901	0.166	0.623
2020-05-21	2020-09-05	0.269	0.585	0.269	0.811
2020-09-06	2020-12-22	0.361	0.732	0.360	1.283
2020-12-23	2021-04-09	0.463	0.317	0.307	0.955

**Table 1.**  $\chi^2/d.o.f$  from fitting to D, <sup>3</sup>He, <sup>4</sup>He individually and fitting to D, <sup>3</sup>He and <sup>4</sup>He simultaneously with with Zhu's model.

begin date	end date	D	<sup>3</sup> He	<sup>4</sup> He	D+ <sup>3</sup> He+ <sup>4</sup> He
2011-05-20	2011-08-30	0.133	1.080	2.570	1.555
2011-08-31	2011-12-16	0.274	1.687	1.665	1.290
2011-12-17	2012-04-02	0.248	0.977	1.747	1.260
2012-04-03	2012-07-19	0.250	0.411	0.966	0.977
2012-07-20	2012-11-04	0.324	1.068	0.974	1.487
2012-11-05	2013-02-20	0.889	1.122	0.872	1.597
2013-02-21	2013-06-08	0.411	0.282	0.702	0.966
2013-06-09	2013-09-24	1.244	0.731	1.986	1.993
2013-09-25	2014-01-10	0.797	1.198	2.435	2.239
2014-02-07	2014-05-25	0.536	1.362	2.757	2.361
2014-05-26	2014-09-10	0.570	0.099	1.163	0.964
2014-09-11	2014-12-27	0.641	0.254	0.962	1.170
2014-12-28	2015-04-14	0.355	0.396	0.298	0.460
2015-04-15	2015-07-31	0.304	0.277	0.394	0.462
2015-08-01	2015-11-16	0.208	0.290	0.120	0.298
2015-11-17	2016-03-03	0.081	0.298	0.285	0.271
2016-03-04	2016-06-19	0.023	0.567	0.368	0.304
2016-06-20	2016-10-05	0.016	0.368	0.315	0.405
2016-10-06	2017-01-21	0.061	0.737	0.625	0.647
2017-01-22	2017-05-09	0.084	1.497	0.472	0.751
2017-05-10	2017-08-25	0.289	0.799	0.807	0.921
2017-08-26	2017-12-11	0.108	0.289	0.150	0.337
2017-12-12	2018-03-29	0.107	0.541	0.240	0.719
2018-03-30	2018-07-15	0.168	0.642	0.568	0.697
2018-07-16	2018-10-31	0.206	0.692	0.640	0.593
2018-11-01	2019-02-16	0.214	0.205	1.041	0.692
2019-03-16	2019-07-01	0.739	1.035	0.515	0.898
2019-07-02	2019-10-17	0.462	0.972	0.561	1.001
2019-10-18	2020-02-02	0.376	0.566	2.459	1.288
2020-02-03	2020-05-20	0.107	0.841	1.558	1.043
2020-05-21	2020-09-05	0.252	0.528	2.065	1.389
2020-09-06	2020-12-22	2.913	0.752	2.257	2.172
2020-12-23	2021-04-09	0.473	0.298	2.367	1.564

**Table 2.**  $\chi^2/d.o.f$  from fitting to D, <sup>3</sup>He, <sup>4</sup>He individually and fitting to D, <sup>3</sup>He and <sup>4</sup>He simultaneously with Cholis' model.

begin date	end date	D	<sup>3</sup> He	<sup>4</sup> He	D+ <sup>3</sup> He+ <sup>4</sup> He
2011-05-20	2011-08-30	0.158	0.923	1.436	1.224
2011-08-31	2011-12-16	0.261	1.171	1.518	1.239
2011-12-17	2012-04-02	0.225	0.817	1.085	1.076
2012-04-03	2012-07-19	0.204	0.337	0.075	0.534
2012-07-20	2012-11-04	0.250	0.917	0.052	0.909
2012-11-05	2013-02-20	0.441	0.353	0.199	0.810
2013-02-21	2013-06-08	0.231	0.569	0.173	0.541
2013-06-09	2013-09-24	0.485	0.254	0.106	0.525
2013-09-25	2014-01-10	0.229	0.285	0.087	0.408
2014-02-07	2014-05-25	0.332	0.207	0.105	0.548
2014-05-26	2014-09-10	0.295	0.433	0.141	0.357
2014-09-11	2014-12-27	0.529	0.228	0.292	0.870
2014-12-28	2015-04-14	0.233	0.455	0.127	0.335
2015-04-15	2015-07-31	0.188	0.793	0.125	0.373
2015-08-01	2015-11-16	0.155	0.588	0.241	0.351
2015-11-17	2016-03-03	0.074	0.289	0.080	0.182
2016-03-04	2016-06-19	0.019	0.191	0.112	0.205
2016-06-20	2016-10-05	0.022	0.085	0.046	0.247
2016-10-06	2017-01-21	0.079	0.386	0.081	0.340
2017-01-22	2017-05-09	0.098	1.382	0.062	0.530
2017-05-10	2017-08-25	0.218	0.083	0.078	0.376
2017-08-26	2017-12-11	0.094	0.090	0.045	0.241
2017-12-12	2018-03-29	0.109	0.214	0.043	0.421
2018-03-30	2018-07-15	0.140	0.221	0.063	0.359
2018-07-16	2018-10-31	0.185	0.353	0.082	0.281
2018-11-01	2019-02-16	0.198	0.189	0.202	0.292
2019-03-16	2019-07-01	0.230	1.226	0.122	0.576
2019-07-02	2019-10-17	0.214	0.206	0.124	0.424
2019-10-18	2020-02-02	0.266	0.231	0.167	0.291
2020-02-03	2020-05-20	0.095	0.590	0.129	0.457
2020-05-21	2020-09-05	0.302	0.323	0.117	0.651
2020-09-06	2020-12-22	0.721	0.762	0.085	0.918
2020-12-23	2021-04-09	0.438	0.142	0.174	0.828

**Table 3.**  $\chi^2/d.o.f$  from fitting to D, <sup>3</sup>He, <sup>4</sup>He individually and fitting to D, <sup>3</sup>He and <sup>4</sup>He simultaneously with Long's model.

begin date	end date	D	<sup>3</sup> He	<sup>4</sup> He	D+ <sup>3</sup> He+ <sup>4</sup> He
2011-05-20	2011-08-30	0.311	1.611	3.223	1.819
2011-08-31	2011-12-16	0.258	2.447	1.609	1.438
2011-12-17	2012-04-02	0.262	2.259	2.627	1.789
2012-04-03	2012-07-19	0.465	5.439	6.016	3.924
2012-07-20	2012-11-04	0.628	9.034	8.132	5.855
2012-11-05	2013-02-20	2.049	9.064	10.426	7.253
2013-02-21	2013-06-08	0.732	4.468	6.548	4.087
2013-06-09	2013-09-24	2.139	9.110	15.245	8.915
2013-09-25	2014-01-10	3.866	14.464	22.243	13.382
2014-02-07	2014-05-25	2.858	10.931	18.440	10.866
2014-05-26	2014-09-10	1.700	4.410	10.228	5.358
2014-09-11	2014-12-27	0.601	3.400	4.519	2.967
2014-12-28	2015-04-14	0.503	0.849	0.791	0.799
2015-04-15	2015-07-31	0.654	1.664	2.565	1.621
2015-08-01	2015-11-16	0.404	0.923	0.905	0.762
2015-11-17	2016-03-03	0.082	0.331	0.324	0.265
2016-03-04	2016-06-19	0.099	0.536	0.376	0.329
2016-06-20	2016-10-05	0.101	0.884	0.315	0.433
2016-10-06	2017-01-21	0.132	1.001	0.594	0.646
2017-01-22	2017-05-09	0.109	1.766	0.503	0.787
2017-05-10	2017-08-25	0.290	2.132	1.625	1.414
2017-08-26	2017-12-11	0.099	0.662	0.417	0.488
2017-12-12	2018-03-29	0.161	1.099	0.402	0.798
2018-03-30	2018-07-15	0.173	1.453	1.053	0.952
2018-07-16	2018-10-31	0.193	1.382	1.094	0.875
2018-11-01	2019-02-16	0.200	1.118	1.142	0.827
2019-03-16	2019-07-01	0.687	1.944	0.786	1.125
2019-07-02	2019-10-17	0.732	2.169	1.119	1.469
2019-10-18	2020-02-02	0.457	1.491	3.595	1.884
2020-02-03	2020-05-20	0.104	2.101	2.084	1.418
2020-05-21	2020-09-05	0.336	1.905	3.345	1.922
2020-09-06	2020-12-22	4.148	1.973	3.304	3.111
2020-12-23	2021-04-09	0.502	1.277	3.404	1.970

**Table 4.**  $\chi^2/d.o.f$  from fitting to D, <sup>3</sup>He, <sup>4</sup>He individually and fitting to D, <sup>3</sup>He and <sup>4</sup>He simultaneously with FFA.

## REFERENCES

- Adriani, O., Barbarino, G. C., Bazilevskaya, G. A., et al. 2011, *Science*, 332, 69, doi: [10.1126/science.1199172](https://doi.org/10.1126/science.1199172)
- Aguilar, M., Ali Cavasonza, L., Alpat, B., et al. 2017, *Phys. Rev. Lett.*, 119, 251101, doi: [10.1103/PhysRevLett.119.251101](https://doi.org/10.1103/PhysRevLett.119.251101)
- Aguilar, M., Ali Cavasonza, L., Alpat, B., et al. 2018a, *Phys. Rev. Lett.*, 121, 051101, doi: [10.1103/PhysRevLett.121.051101](https://doi.org/10.1103/PhysRevLett.121.051101)
- Aguilar, M., Cavasonza, L. A., Ambrosi, G., et al. 2018b, *Phys. Rev. Lett.*, 121, 051102, doi: [10.1103/PhysRevLett.121.051102](https://doi.org/10.1103/PhysRevLett.121.051102)
- Aguilar, M., et al. 2021a, *Phys. Rev. Lett.*, 127, 271102, doi: [10.1103/PhysRevLett.127.271102](https://doi.org/10.1103/PhysRevLett.127.271102)
- Aguilar, M., Ali Cavasonza, L., Ambrosi, G., et al. 2021b, *Physics Reports*, 894, 1, doi: <https://doi.org/10.1016/j.physrep.2020.09.003>
- Aguilar, M., Cavasonza, L. A., Ambrosi, G., et al. 2022, *Phys. Rev. Lett.*, 128, 231102, doi: [10.1103/PhysRevLett.128.231102](https://doi.org/10.1103/PhysRevLett.128.231102)
- Aguilar, M., Alpat, B., Ambrosi, G., et al. 2024, *Phys. Rev. Lett.*, 132, 261001, doi: [10.1103/PhysRevLett.132.261001](https://doi.org/10.1103/PhysRevLett.132.261001)
- . 2025, *Phys. Rev. Lett.*, 134, 051001, doi: [10.1103/PhysRevLett.134.051001](https://doi.org/10.1103/PhysRevLett.134.051001)
- Ambrosi, G., An, Q., Asfandiyarov, R., et al. 2017, *Nature*, 552, 63, doi: [10.1038/nature24475](https://doi.org/10.1038/nature24475)
- Blasi, P. 2013, *The Astronomy and Astrophysics Review*, 21, 70, doi: [10.1007/s00159-013-0070-7](https://doi.org/10.1007/s00159-013-0070-7)
- Cholis, I., Hooper, D., & Linden, T. 2016, *Phys. Rev. D*, 93, 043016, doi: [10.1103/PhysRevD.93.043016](https://doi.org/10.1103/PhysRevD.93.043016)
- Cholis, I., Hooper, D., & Linden, T. 2022, *JCAP*, 10, 051, doi: [10.1088/1475-7516/2022/10/051](https://doi.org/10.1088/1475-7516/2022/10/051)
- Cooke, R. J., Pettini, M., & Steidel, C. C. 2018, *The Astrophysical Journal*, 855, 102, doi: [10.3847/1538-4357/aaab53](https://doi.org/10.3847/1538-4357/aaab53)
- Corti, C., Bindi, V., Consolandi, C., et al. 2019a, <https://arxiv.org/abs/1910.00027>
- Corti, C., Bindi, V., Consolandi, C., & Whitman, K. 2016, *Astrophys. J.*, 829, 8, doi: [10.3847/0004-637X/829/1/8](https://doi.org/10.3847/0004-637X/829/1/8)
- Corti, C., Potgieter, M. S., Bindi, V., et al. 2019b, *The Astrophysical Journal*, 871, 253, doi: [10.3847/1538-4357/aafac4](https://doi.org/10.3847/1538-4357/aafac4)
- Cui, M.-Y., Yuan, Q., Tsai, Y.-L. S., & Fan, Y.-Z. 2017, *Phys. Rev. Lett.*, 118, 191101, doi: [10.1103/PhysRevLett.118.191101](https://doi.org/10.1103/PhysRevLett.118.191101)
- Di Felice, V., Munini, R., Vos, E. E., & Potgieter, M. S. 2017, *Astrophys. J.*, 834, 89, doi: [10.3847/1538-4357/834/1/89](https://doi.org/10.3847/1538-4357/834/1/89)
- Gamerman, D. 1997, *Markov Chain Monte Carlo: Stochastic Simulation for Bayesian Inference* (London: Chapman and Hall)
- Gieseler, J., Heber, B., & Herbst, K. 2017, *Journal of Geophysical Research (Space Physics)*, 122, 10, doi: [10.1002/2017JA024763](https://doi.org/10.1002/2017JA024763)
- Gleeson, L. J., & Axford, W. I. 1967, *Astrophys. J. Lett.*, 149, L115, doi: [10.1086/180070](https://doi.org/10.1086/180070)
- . 1968, *Astrophys. J.*, 154, 1011, doi: [10.1086/149822](https://doi.org/10.1086/149822)
- Lafferty, G. D., & Wyatt, T. R. 1995, *Nuclear Instruments and Methods in Physics Research A*, 355, 541, doi: [10.1016/0168-9002\(94\)01112-5](https://doi.org/10.1016/0168-9002(94)01112-5)
- Lavalle, J., & Salati, P. 2012, *Comptes Rendus Physique*, 13, 740, doi: [10.1016/j.crhy.2012.05.001](https://doi.org/10.1016/j.crhy.2012.05.001)
- Lewis, A., & Bridle, S. 2002, *Phys. Rev. D*, 66, 103511, doi: [10.1103/PhysRevD.66.103511](https://doi.org/10.1103/PhysRevD.66.103511)
- Li, J.-T., Beacom, J. F., & Peter, A. H. G. 2022, *The Astrophysical Journal*, 937, 27, doi: [10.3847/1538-4357/ac8cf3](https://doi.org/10.3847/1538-4357/ac8cf3)
- Liu, J., Yuan, Q., Bi, X.-J., Li, H., & Zhang, X. 2012, *Physical Review D*, 85, doi: [10.1103/physrevd.85.043507](https://doi.org/10.1103/physrevd.85.043507)
- Long, W.-C., & Wu, J. 2024, *Phys. Rev. D*, 109, 083009, doi: [10.1103/PhysRevD.109.083009](https://doi.org/10.1103/PhysRevD.109.083009)
- Luo, X., Potgieter, M. S., Bindi, V., Zhang, M., & Feng, X. 2019, *The Astrophysical Journal*, 878, 6, doi: [10.3847/1538-4357/ab1b2a](https://doi.org/10.3847/1538-4357/ab1b2a)
- Moskalenko, I. V., & Strong, A. W. 1998, *Astrophys. J.*, 493, 694, doi: [10.1086/305152](https://doi.org/10.1086/305152)
- Parker, E. N. 1965, *Planet. Space Sci.*, 13, 9, doi: [10.1016/0032-0633\(65\)90131-5](https://doi.org/10.1016/0032-0633(65)90131-5)
- Potgieter, M. S. 2013, *Living Reviews in Solar Physics*, 10, 3, doi: [10.12942/lrsp-2013-3](https://doi.org/10.12942/lrsp-2013-3)
- Potgieter, M. S., Vos, E. E., Boezio, M., et al. 2014, *SoPh*, 289, 391, doi: [10.1007/s11207-013-0324-6](https://doi.org/10.1007/s11207-013-0324-6)
- Potgieter, M. S., Vos, E. E., Munini, R., Boezio, M., & Di Felice, V. 2015, *Astrophys. J.*, 810, 141, doi: [10.1088/0004-637X/810/2/141](https://doi.org/10.1088/0004-637X/810/2/141)
- Shen, Z., Yang, H., Zuo, P., et al. 2021, *Astrophys. J.*, 921, 109, doi: [10.3847/1538-4357/ac1fe8](https://doi.org/10.3847/1538-4357/ac1fe8)
- Siruk, S., Kuznetsov, A., Mayorov, A., & Yulbarisov, R. 2024, *Advances in Space Research*, 74, 1978, doi: <https://doi.org/10.1016/j.asr.2024.05.050>
- Song, X., Luo, X., Potgieter, M. S., Liu, X., & Geng, Z. 2021, *The Astrophysical Journal Supplement Series*, 257, 48, doi: [10.3847/1538-4365/ac281c](https://doi.org/10.3847/1538-4365/ac281c)
- Stone, E. C., Cummings, A. C., Heikkilä, B. C., & Lal, N. 2019, *Nature Astronomy*, 3, 1013, doi: [10.1038/s41550-019-0928-3](https://doi.org/10.1038/s41550-019-0928-3)

- Stone, E. C., Cummings, A. C., McDonald, F. B., et al. 2013, *Science*, 341, 150, doi: [10.1126/science.1236408](https://doi.org/10.1126/science.1236408)
- Strong, A. W., Moskalenko, I. V., & Ptuskin, V. S. 2007, *Annual Review of Nuclear and Particle Science*, 57, 285, doi: [10.1146/annurev.nucl.57.090506.123011](https://doi.org/10.1146/annurev.nucl.57.090506.123011)
- Sun, X., Hoeksema, J. T., Liu, Y., & Zhao, J. 2015, *Astrophys. J.*, 798, 114, doi: [10.1088/0004-637X/798/2/114](https://doi.org/10.1088/0004-637X/798/2/114)
- Tomassetti, N., Barão, F., Bertucci, B., et al. 2018, *Phys. Rev. Lett.*, 121, 251104, doi: [10.1103/PhysRevLett.121.251104](https://doi.org/10.1103/PhysRevLett.121.251104)
- Usoskin, I. G., Bazilevskaya, G. A., & Kovaltsov, G. A. 2011, *Journal of Geophysical Research (Space Physics)*, 116, A02104, doi: [10.1029/2010JA016105](https://doi.org/10.1029/2010JA016105)
- Wang, B.-B., Bi, X.-J., Fang, K., Lin, S.-J., & Yin, P.-F. 2022, *Phys. Rev. D*, 106, 063006, doi: [10.1103/PhysRevD.106.063006](https://doi.org/10.1103/PhysRevD.106.063006)
- Yuan, Q., & Fan, Y.-Z. 2024, *The Astrophysical Journal Letters*, 974, L14, doi: [10.3847/2041-8213/ad7e2c](https://doi.org/10.3847/2041-8213/ad7e2c)
- Zhu, C.-R. 2024, *The Astrophysical Journal*, 975, 270, doi: [10.3847/1538-4357/ad794b](https://doi.org/10.3847/1538-4357/ad794b)
- Zhu, C.-R., Cui, M.-Y., Xia, Z.-Q., et al. 2022, *Phys. Rev. Lett.*, 129, 231101, doi: [10.1103/PhysRevLett.129.231101](https://doi.org/10.1103/PhysRevLett.129.231101)
- Zhu, C.-R., & Duan, K.-K. 2025, Forecasting of the time-dependent fluxes of antiprotons in the AMS-02 era. <https://arxiv.org/abs/2501.12625>
- Zhu, C.-R., & Wang, M.-J. 2025, *The Astrophysical Journal*, 980, 116, doi: [10.3847/1538-4357/adacd8](https://doi.org/10.3847/1538-4357/adacd8)
- Zhu, C.-R., Yuan, Q., & Wei, D.-M. 2018, *Astrophys. J.*, 863, 119, doi: [10.3847/1538-4357/aacff9](https://doi.org/10.3847/1538-4357/aacff9)
- . 2021, *Astropart. Phys.*, 124, 102495, doi: [10.1016/j.astropartphys.2020.102495](https://doi.org/10.1016/j.astropartphys.2020.102495)